RSC Advances

This is an *Accepted Manuscript*, which has been through the Royal Society of Chemistry peer review process and has been accepted for publication.

Accepted Manuscripts are published online shortly after acceptance, before technical editing, formatting and proof reading. Using this free service, authors can make their results available to the community, in citable form, before we publish the edited article. This *Accepted Manuscript* will be replaced by the edited, formatted and paginated article as soon as this is available.

You can find more information about *Accepted Manuscripts* in the Information for Authors.

Please note that technical editing may introduce minor changes to the text and/or graphics, which may alter content. The journal's standard Terms & Conditions and the Ethical guidelines still apply. In no event shall the Royal Society of Chemistry be held responsible for any errors or omissions in this *Accepted Manuscript* or any consequences arising from the use of any information it contains.

ROYAL SOCIETY OF CHEMISTRY

www.rsc.org/advances

CREATED USING THE RSC COMMUNICATION TEMPLATE (VER. 3.1) - SEE WWW.RSC.ORG/ELECTRONICFILES FOR DETAILS

ARTICLE TYPE www.rsc.org/xxxxxx | XXXXXXXX

Carbon-doped Titania Flakes with Octahedral Bipyramid Skeleton Structure for the Visible-light Photocatalytic Mineralization of Ciprofloxacin†

Jian-Wen Shi,*[a] Zhenyu Wang,[a] Chi He, [b] Guodong Li [c] and Chunming Niu*[a]

Received (in XXX, XXX) Xth XXXXXXXXX 20XX, Accepted Xth XXXXXXXXX 20XX
First published on the web Xth XXXXXXXXX 20XX
DOI: 10.1039/b000000x

Pharmaceutical and Personal Care Products (PPCPs) are emerging contaminants, which can affect water quality and potentially impact drinking water supplies, ecosystem and human health. A novel and unique structure, octahedral bipyramid skeleton, assembled by three pieces of carbon self-doped TiO_2 flakes with exposed {001} facets was explored for the first time to mineralize ciprofloxacin, one of PPCPs. The results demonstrated that the obtained C-doped TiO_2 flakes presented higher visible-light photocatalytic activity in comparison with the reported C-doped TiO_2 sheets with exposed {001} facets, which can be ascribed to the narrower band gap, the higher percentage of the exposed {001} facts, the larger specific surface area, and the unique octahedral bipyramid skeleton structure.

Pharmaceutical and Personal Care Products (PPCPs) are emerging contaminants, which have attracted increasing concerns in recent years.[1] Owing to their persistence against biological degradation and natural attenuation, conventional wastewater treatment technologies, such as activated sludge and filtration, cannot efficiently remove PPCPs from water.[2] Therefore, effective alternative technologies are highly desired to deal with the pollution resulted from PPCPs.

As an important semiconductor material, titania (TiO_2) has been most widely investigated in the past decades due to its great potential in the photocatalytic mineralization of organic pollutants.[3] However, the large band gap and the rapid recombination of photoexcited electrons and holes limit its catalytic activity and practical application.[4] It has been confirmed from both theory and experiment that the {001} facets of anatase TiO_2 are highly reactive, therefore the exposure of {001} facets is considered as an effective approach to improve the photocatalytic activity of TiO_2.[5] Even more inspiringly, recent studies show crystal facets play an important role in the separation of photo-generated electron-hole pairs.[6] Owing to the difference of energy levels of crystal facets, the photo-generated electrons and holes can be separated between the different crystal facets, which can efficiently prevent their recombination to improve catalytic activity of semiconductors, such as $BiVO_4$, anatase TiO_2. However, the photocatalytic activity of TiO_2 crystals with high reactive {001} facets is still limited owing to its large band gap.[7] For enhancing the utilizing efficiency of solar light, visible light responsive TiO_2 crystals with high reactive {001} facets are highly desired.

It is well known that ion doping, especially nonmetal doping (N,[8] C,[9] etc.), is a very promising strategy for extending the photo-response of TiO_2 from UV to visible light region. For example, Khan et al. found C-doped TiO_2 could absorb light at wavelengths up to 535 nm.[9] Recently, nonmetal doped TiO_2 crystals (e.g., N, S, F) with exposed {001} facets have been successfully synthesized by treating corresponding titanium precursor (e.g., TiN, TiS_2, $TiOF_2$),[10] and their visible-light photocatalytic activities have been demonstrated. Although TiC has been used as precursor to prepare C-doped TiC photocatalysts, these resultants are no exposed {001} facets.[11] Until recently, C-doped TiO_2 sheets (CTS) with exposed {001} facets were successfully synthesized by the hydrothermal treatment of TiC in the presence of HF.[12] Furthermore, it was demonstrated that the resulting CTS exhibited much higher photocatalytic activity than that of the C-doped TiO_2 particles due to the presence of exposed {001} facets. However, the obtained CTS exists in an aggregated form with the size of several micrometers, which inevitably results in its low specific surface areas (12 m^2/g).[12] Therefore, further studies on C-doped TiO_2 with exposed {001} facets are highly desirable to further enhance its visible-light photocatalytic performance.

Herein we reported a novel carbon self-doped TiO_2 flakes (CTF) with dominant {001} facets derived from TiC powder. These TiO_2 flakes have square outline with the micrometer-sized length and nanometer-sized thickness. Furthermore, these flakes vertically intercross each other and orient the diagonal of square to construct octahedral bipyramid skeleton structure. Compared with CTS with exposed {001} facets, the as-prepared CTF with dominant {001} facets presented higher photocatalytic activity under visible light irradiation.

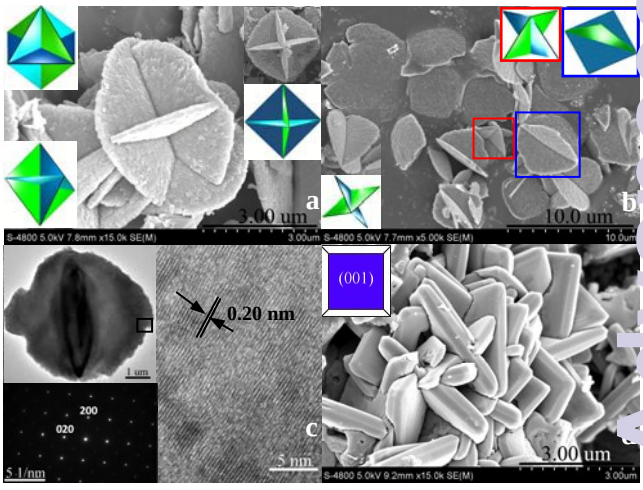

Fig. 1. (a and b) SEM of CTF (insets are the corresponding structure schemes); (c) HRTEM of CTF (insets are the TEM and SAED pattern of CTF, respectively); (d) SEM of CTS (inset is a geometrical model of the anatase TiO_2 single crystal with exposed {001} facets).

RSC Advances Accepted Manuscript

CTF with dominant {001} facets were prepared by hydrothermal treatment of TiC powder in a HF-HNO_3 mixed aqueous solution. TiC powder was employed as both TiO_2 precursor and carbon dopant source. HF was used as facet controlling reagent, and HNO_3 was utilized as reactant to react with TiC. For comparison, CTS with exposed {001} facets were also prepared based on the previous work.[12] The detailed synthesis processes of CTF and CTS can be found in the ESI†.

Fig. 1a shows the SEM image of the as-prepared CTF sample. These titania flakes present square outline with the side length of about 4.0 μm and the thickness of approximately 100 nm, and the percentage of {001} facets is estimated to be ca. 95.6%. A lot of trench-like structures can be found on the surface of TiO_2 flakes (Fig. S1, ESI†), which helps to improve the specific surface area of sample. It can be found that the octahedral bipyramid skeleton structure consisted of three pieces of TiO_2 flakes has formed. The three pieces of TiO_2 flakes vertically intercross each other and orient the diagonal of the square to assemble into one octahedral bipyramid skeleton structure, as illustrated in the inset at the upper left corner in Fig. 1a (the corresponding structure scheme of the SEM viewed from the similar angle is displayed in the lower left corner in Fig. 1a). This octahedral bipyramid skeleton structure can be further confirmed by the SEM image taken from a more appropriate angle of view (the inset at the upper right corner in Fig. 1a, and the corresponding structure scheme can be found right under of this inset). We also found some half-baked octahedral bipyramid skeleton structures comprised two pieces of TiO_2 flakes which vertically intercross each other and orient the diagonal of the square (Fig. 1b). In addition, some single TiO_2 flakes can also be discovered. The TEM image also clearly displays this perpendicularly intersecting sheet structure. As shown in the inset at the upper left corner in Fig. 1c, one flake grown vertically on the other square sheet along the diagonal direction. The HRTEM image (Fig. 1c, recorded from the black square in TEM image) clearly shows the continuous atomic planes with a lattice spacing of 0.20 nm, corresponding to the {200} planes of anatase TiO_2 crystals,[13] which confirms the exposed crystal facet is the {001} facet (more HRTEM images can be found in Fig. S2, ESI†). The SAED pattern (the inset at the lower left corner in Fig. 1c) displays the diffraction spots of the [001] zone, confirming that the as-prepared TiO_2 sheet is a single crystal. As a comparison, the SEM image of the CTS sample is presented in Fig. 1d. The TiO_2 sheets consist of well-defined plate-shaped structures with a square outline, and the two flat and square surfaces can be assigned to {001} and the eight isosceles trapezoidal surfaces are {101} facets of the anatase TiO_2 crystal,[5a] as illustrated in the inset in Fig. 1d. The side length and the thickness of TiO_2 sheets are about 3.4 μm and 500 nm, respectively, and the percentage of {001} facets is estimated to be ca. 76.1%. It should be noted that these sheets intercross each other without obvious regularity to form large blocks, which is disadvantageous to the enhancement of the specific surface area of sample, and is also harmful to the exposure of {001} facets to inter-medium.

The crystal structures of CTF and CTS were investigated with X-ray diffraction analysis (XRD). As shown in Fig. 2a, all the diffraction peaks of CTS can be assigned to anatase TiO_2 (JCPDS: 00-021-1272), implying that TiC precursor has been completely transformed into anatase phase (the XRD pattern of TiC precursor is showed in Fig. S3, ESI†). Both anatase TiO_2 (99.5%) and rutile TiO_2 (0.5%, JCPDS: 01-078-1508) are detected in the CTF sample. This mixed crystal phase is helpful to improve the photocatalytic activity for the reduction of electron-hole pair recombination rate resulted from the hetero-junction effect. The XPS survey scan of CTF (Fig. S4a, ESI†) shows only the elements of Ti, O, C and F are observed. The binding energies of Ti $2p_{3/2}$ and Ti $2p_{1/2}$ are 459.02 and 464.67 eV (space 5.65 eV), respectively (Fig. S5, ESI†), indicating that the oxidation state of the Ti element is positive tetravalent (Ti^{4+}).[14] The binding energy of F 1s is 684.6 eV (Fig. S6, ESI†), which is a typical value from F^- for fluorated TiO_2 system, such as Ti–F species,[5a] No fluorine ions in the crystal lattice (BE=688.0~689.0 eV) were observed, implying the oxygen in TiO_2 lattice was not substituted by fluorine.[15] Fig. 2b displays the high-resolution C1s XPS spectrum of CTF, which can be fitted as three peaks at binding energies of 284.7, 286.0 and 288.7 eV, respectively, indicating that three different chemical environments of carbon exist in the sample. Furthermore, the peak at a binding energy value of 281.8 eV (C1s peak of TiC)[11c,16] is absent in the case of CTF, implying a complete conversion of TiC into C-doped TiO_2. The strong peak at 284.7 eV is ascribed to the residual elemental carbon (BE = 284.6 eV),[17] which can act as photo-sensitizer to promote visible light response of CTF.[17] The peak at 286.0 eV is usually assigned to C–O-like species.[11d,18] The peak at 288.7 eV can be attributed to the carbonate species, which were formed during the hydrothermal treatment of TiC powder due to the incorporation of carbon atoms into the interstitial positions of the TiO_2 lattice.[12,16,19] Based on the above observations, it is confirmed that carbon self-doping occurred during the hydrothermal treatment of TiC powder, which can lead to the formation of additional localized states above the valence band (VB) top of TiO_2, accordingly narrow the band gap of TiO_2 and promote the visible light response.[20] Fig. 2c displays the UV-Vis absorption spectra of CTF, CTS and P25, together with the color pictures of the three samples (Fig. S7, the UV-Vis absorption spectra of TiC precursor is showed in Fig. S8, ESI†). Compared with P25, CTF and CTS samples show two distinguishing features due to C-doping: 1) the absorption edge at about 400 nm shows an obvious red shift, and 2) the absorbance in the whole visible region is improved. The two features further confirm that carbon atoms have been successfully doped into TiO_2 lattice. Furthermore, the red shift and the absorbance in visible region in CTF sample are more significant than that in CTS sample, which can be attributed to the fact that the surface fluorination is beneficial for doping TiO_2 with carbon.[12,21] These rules are in a good agreement with the above presented XPS analysis. To confirm the red shift and the absorbance in visible region in theory, the first-principle density functional theory (DFT) was used to calculate the effect of C-doping on the band gap of TiO_2 (The supercell model for calculation is shown in Fig. S9, ESI†). As shown in Fig. S10 (ESI†), the calculated band gap of un-doped anatase TiO_2 is about 3.24 eV with LDA+U correction, which is very close to the experimental value of 3.20 eV. For the CTF, C-doping narrows TiO_2 band gap from 3.24 eV to about 2.78 eV, and some impurity states occur in the middle of valence band maximum and conduction band minimum, which narrow the intrinsic gap of TiO_2 and lead to the red shift of absorption edge and the stronger visible light absorption, which can be further confirmed by our calculated optical absorption spectra (Fig. S11, ESI†). Fig. 2d shows the nitrogen adsorption and desorption isotherms of CTF and CTS. Both of them present type IV isotherm with a hysteresis, indicating the presence of mesopores.[22] The BJH pore diameter distribution curve of CTS obtained from the desorption branch has a sharp maximum at about 3.9 nm, which can be ascribed to mesopores in the large blocks formed from those intersectional sheets, as indicated in SEM (Fig. 1d). For CTF sample, the peak is moved to approximately 5.2 nm, which can be attributed to those trench-like structures formed on the surface of flakes. The

RSC Advances Accepted Manuscript

This journal is © The Royal Society of Chemistry [year]

BET specific surface areas (S_{BET}) of CTS and CTF are 8.68 and 28.42 m^2/g, respectively. The S_{BET} of CTF is almost 3.27 times than that of CTS due to the thinness and the trench-like structures, which implies CTF has superior adsorption property.

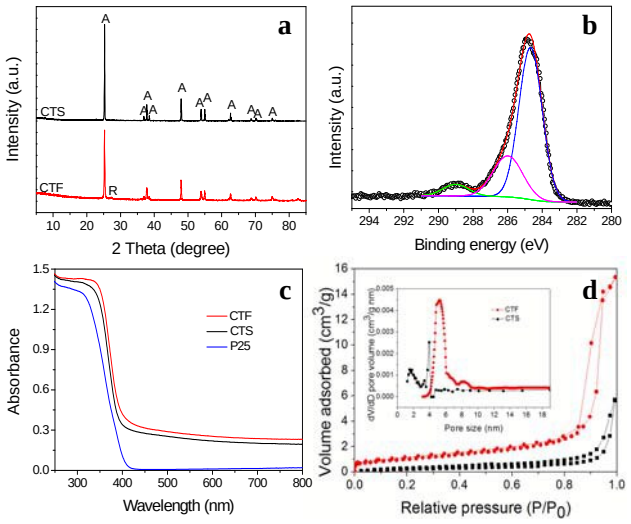

Fig. 2. XRD patterns of CTF and CTS (a), high-resolution C1s XPS spectrum of CTF (b), UV-visible spectra of CTF, CTS and P25 (c), nitrogen adsorption and desorption isotherms and pore diameter distribution curves of CTF and CTS (d).

In order to compare the difference of the photocatalytic activity between the two samples (CTF and CTS), photocatalytic mineralization of ciprofloxacin (abbreviated as CIP, one of PPCPs) solution under visible light irradiation (λ > 420 nm) by using them as photocatalysts was carried out in a photo reaction system illustrated in Fig. S12 (ESI†). For comparison, the photocatalytic activity of P25 was tested together. As shown in Fig. 3a, the blank experiment shows CIP is difficult to be photo-mineralized in the absence of catalyst. P25 also shows non-activity for the mineralization of CIP under visible light. Compared with P25, the photocatalytic activity of CTS is improved due to the doping of carbon, and about 35.0% of CIP is mineralized in 6 h. The photocatalytic activity of CTF is further enhanced in comparison with that of CTS, and about 70.0% of CIP is mineralized within the same time (6 h). To understand the reaction mechanism of CIP mineralization, we applied the pseudo-first order model as expressed by the equation $ln(TOC_0/TOC) = kt$, which is generally used for photocatalytic mineralization process,[23] to treat the experimental data. The straight line fitting shows that the reaction kinetics is first order indeed (Fig. S13). The reaction rate constants deduced from the slopes are 0.000287, 0.07942 and 0.18937 h^{-1} for P25, CTS and CTF, respectively. The rate constant corresponding to the visible light photocatalytic activity is enhanced 2.38 times from CTS to CTF, which can be attributed to the synergic effects of several factors, such as the narrowing of band gap due to the carbon self-doping, the higher percentage of the exposed {001} facts, the larger specific surface area owing to the thinness and the trench-like structures. In addition, the unique octahedral bipyramid skeleton structure can avoid the compact stack of TiO_2 flakes. As a result, the supporting spaces can offer an excellent pathway facilitating the transmission and diffusion of CIP and H_2O molecules, which is very helpful for the improvement of photocatalytic mineralization efficiency. From the viewpoint of practical application, the favorable recycling and the stability of catalyst are very important. Due to relatively larger size compared with nano-titania particles, CTF pieces are very easy to be separated from treated water by precipitating in a quiescent condition. To test the stability of CTF, recycle experiments on photocatalytic mineralization of CIP by CTF were carried out six times. As shown in Fig. 3b, the efficiencies of photocatalytic mineralization are almost no decline under repeated application. Therefore, the as-prepared CTF is a favorable recycling, stable and high visible-light activity photocatalyst, and it is expected to be useful in environment remediation and energy conversion such as water splitting and solar cell.

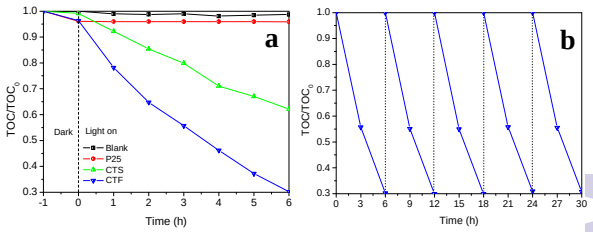

Fig. 3. (a) Photocatalytic mineralization of CIP solution over different photocatalysts under visible light irradiation (λ > 420 nm); (b) Cycling test results of photocatalytic activity (CIP mineralization) of CTF under visible light irradiation.

In summary, visible-light-responsive carbon self-doped TiO_2 flake with octahedral bipyramid skeleton structure and exposed {001} facets was successfully prepared by hydrothermal treatment of TiC powder in a HF-HNO_3 mixed aqueous solution. These flakes have square outline with the micrometer-sized length and nanometer-sized thickness, and they vertically intercross each other and orient the diagonal of square. Compared with reported C-doped TiO_2 sheets with exposed {001} facets, the obtained catalyst presented higher visible-light photocatalytic activity, which can be attributed to the narrower band gap due to C-doping, the higher percentage of the exposed {001} facts, the larger specific surface area. In addition, the unique octahedral bipyramid skeleton structure provided a positive effect on the improvement of photocatalytic mineralization efficiency due to the fact that this structure can avoid the compact stack of TiO_2 flakes. Work on further optimizing the photocatalytic activity of CTF and the formation mechanism of the unique structure, octahedral bipyramid skeleton, is underway.

This work was sponsored by the National Natural Science Fund Committee-Baosteel Group Corporation Steel Joint Research Fund (U1460105), Natural Science Foundation of Shaanxi Province (2015JM2055), the Fundamental Research Funds for the Central Universities (2015gjhz06) and the Opening Project of State Key Laboratory of Inorganic Synthesis and Preparative Chemistry (2015-14). The authors thank Prof. Y. H. Chen for providing a SGI working station and the CASTEP code, and thank Ms. Juan Feng, Ms. Lu Lu and Mr. Chuansheng Ma for their helps with SEM and TEM characterization carried out at the International Center for Dielectric Research (ICDR), Xi'an Jiaotong University.

Notes and references

[a] *Center of Nanomaterials for Renewable Energy, State Key Laboratory of Electrical Insulation and Power Equipment, School of Electrical Engineering, Xi'an Jiaotong University, Xi'an 710049, China. Fax/Tel: +86 29 83395372; E-mail: jianwen.shi@mail.xjtu.edu.cn; cniu@mail.xjtu.edu.cn*

RSC Advances Accepted Manuscript

[b] *Department of Environmental Science and Engineering, School of Energy and Power Engineering, Xi'an Jiaotong University, Xi'an 710049, China.*
[c] *State Key Laboratory of Inorganic Synthesis and Preparative Chemistry, College of Chemistry, Jilin University, Changchun 130012, China*

† Electronic Supplementary Information (ESI) available: Details of experimental procedures, characterization, photocatalytic activity test, calculation methods and details, and supporting images. See DOI: 10.1039/b000000x/

1 J. B. Ellis, Environ. Poll. 2006,**144**, 184.
2 *(a)* S. Esplugas, D. M. Bila, L. G. T. Krause and M. Dezotti, *J. Hazard. Mat*. 2007, **149**, 631; *(b)* J.-W. Shi, Z. Wang, C. He, H. Wang, J.-W. Chen, M.-L. Fu, G. Li and C. Niu, *J. Mol. Catal. A* 2015, **399**, 79; *(c)* J.-W. Shi, C. Xie, C. He, C. Liu, C. Gao, S. Yang, J.-W. Chen and G. Li, *Catal. Commu*n. 2015, **66**, 46.
3 *(a)* M. A. Fox and M. T. Dulay, *Chem. Rev*., 1993, **93**, 341; *(b)* M. R. Hoffmann, S. T. Martin, W. Choi and D. W. Bahnemannt, *Chem. Rev*., 1995, **95**, 69; *(c)* T. Tachikawa and T. Majima, *Chem. Soc. Rev*., 2010, **39**, 4802; *(d)* S. Y. Reece, J. A. Hamel, K. Sung, T. D. Jarvi, A. J. Esswein, J. J. H. Pijpers and D. G. Nocera, *Science*, 2011, **334**, 645; *(e)* X. Lang, X. Chen and J. Zhao, *Chem. Soc. Rev*., 2014, **43**, 473.
4 *(a)* X. Chen and S. S. Mao, *Chem. Rev*., 2007, **107**, 2891; *(b)* M. N. Chong, B. Jin, C. W.K. Chow and C. Saint, *Water Res.*, 2010, **44**, 2997; *(c)* M. Pelaez, N. T. Nolan, S. C. Pillai, M. K. Seery, P. Falaras, A. G. Kontos, P. S.M. Dunlop, J. W.J. Hamilton, J. A. Byrne, K. O'Shea, M. H. Entezari and D. D. Dionysiou, *Appl. Catal. B*, 2012, **125**, 331; *(d)* L. Gomathi Devi and R. Kavitha, *Appl. Catal. B*, 2013, **140–141**, 559.
5 *(a)* H. G. Yang, C. H. Sun, S. Z. Qiao, J. Zou, G. Liu, S. C. Smith, H. M. Cheng and G. Q. Lu, *Nature*, 2008, **53**, 638; *(b)* D. Zhang, G. Li, X. Yang and J. C. Yu, *Chem. Commun*., 2009, **45**, 4381; *(c)* M. Liu, L. Piao, L. Zhao, S. Ju, Z. Yan, T. He, C. Zhou and W. Wang, *Chem. Commun*., 2010, **46**, 1664; *(d)* S. Liu, J. Yu and M. Jaroniec, *Chem. Mater*., 2011, **23**, 4085; *(e)* Y. Yu, C. Cao, W. Li, P. Li, J. Qu and W. Song, *Nano Res*., 2012, **5**, 434.
6 *(a)* R. Li, F. Zhang, D. Wang, J. Yang, M. Li, J. Zhu, X. Zhou, H. Han and C. Li, *Nat. Commun.*, 2013, **4**, 1432; *(b)* C. Liu, X. Han, S. Xie, Q. Kuang, X. Wang, M. Jin, Z. Xie, and L. Zheng, *Chem. Asian J*., 2013, **8**, 282.
7 *(a)* U. Diebold, *Surf. Sci. Rep.*, 2003, **48**, 53; *(b)* W.-J. Ong, L.-L. Tan, S.-P. Chai, S.-T. Yong and A. R. Mohamed, *Nanoscale*, 2014, **6**, 1946.
8 R. Asahi, T. Morikawa, T. Ohwaki, K. Aoki and Y. Taga, *Science*, 2001, **293**, 269.
9 S. U. M. Khan, M. Al-Shahry and W. B. Ingler Jr, *Science*, 2002, **297**, 2243.
10 *(a)* G. Liu, H. G. Yang, X. Wang, L. Cheng, J. Pan, G. Q. Lu and H.-M. Cheng, *J. Am. Chem. Soc*., 2009, **131**, 12868; *(b)* G. Liu, C. Sun, S. C. Smith, L. Wang, G. Q. M. Lu and H. M. Cheng, *J. Colloid Interface Sci.*, 2010, **349**, 477; *(c)* X. Zong, Z. Xing, H. Yu, Z. Chen, F. Tang, J. Zou, G. Q. Lu and L. Wang, *Chem. Commun*., 2011, **47**, 11742.
11 *(a)* M. Shen, Z. Wu, H. Huang, Y. Du, Z. Zou and P. Yang, *Mater. Lett.*, 2006, **60**, 693; *(b)* X. Cui, H. Gu, J. Lu, J. Shen and Z. Zhang, *J. Nanosci. Nanotechno.*, 2007, **7**, 3140; *(c)* D. E. Gu, Y. Lu, B. C. Yang and Y. D. Hu, *Chem. Commun.*, 2008, **44**, 2453; *(d)* V. Kiran and S. Sampath, *ACS Appl. Mater. Interfaces*, 2012, **4**, 3818; *(e)* V. Kiran and S. Sampath, *Nanoscale*, 2013, **5**, 10646; *(f)* D.-L. Shieh, S.-J. Huang, Y.-C. Lin, Y.-S. Lin, J.-L. Lin, T.-F. Yeh and H. Teng, *Micropor. Mesopor. Mat.*, 2013, **167**, 237.
12 J. Yu, G. Dai, Q. Xiang and M. Jaroniec, *J. Mater. Chem.*, 2011, **21**, 1049.
13 *(a)* Y. W. Jun, M. F. Casula, J.-H. Sim, S. Y. Kim, J. Cheon and A. P. Alivisatos, *J. Am. Chem. Soc.*, 2003, **125**, 15981; *(b)* H. G. Yang, G. Liu, S. Z. Qiao, C. H. Sun, Y. G. Jin, S. C. Smith, J. Zou, H. M. Cheng and G. Q. Lu, *J. Am. Chem. Soc.*, 2009, **131**, 4078.
14 *(a)* X. W. Lou and H. C. Zeng , *J. Am. Chem. Soc*., 2003, **125**, 2697; *(b)* X. Zhao, W. Jin, J. Cai, J. Ye, Z. Li, Y. Ma, J. Xie and L. Qi, *Adv. Funct. Mater*., 2011, **21**, 3554.
15 *(a)* J. H. Pan, X. Zhang, A. J. Du, D. D. Sun and J. O. Leckie, *J. Am. Chem. Soc*., 2008, **130**, 11256; *(b)* H. Park and W. Choi, *J. Phys. Chem. B*, 2004, **108**, 4086; *(c)* H. Zhang, P. Liu, F. Li, H. Liu, Y. Wang, S. Zhang, M. Guo, H. Cheng and H. Zhao, *Chem. Eur. J.*, 2011, **17**, 5949.
16 V. Kiran, S. B. Kalidindi, B. R. Jagirdar and S. Sampath, *Electrochim. Acta*, 2011, **56**, 10493.
17 *(a)* F. Dong, H. Wang and Z. Wu, *J. Phys. Chem. C*, 2009, **113**, 16717; *(b)* J. A. Rengifo-Herrera, J. Kiwi and C. Pulgarin, *J. Photochem. Photobiol. A*, 2009, **205**, 109; *(c)* L. Zhao, X. Chen, X. Wang, Y. Zhang, W. Wei, Y. Sun, M. Antonietti and M.-M. Titirici, *Adv. Mater.*, 2010, **22**, 3317; *(d)* X. Yang, C. Cao, K. Hohn, L. Erickson, R. Maghirang, D. Hamal and K. Klabunde, *J. Catal.*, 2007, **252**, 296.
18 Y. Cong, X. Li, Y. Qin, Z. Dong, G. Yuan, Z. Cui and X. Lai, *Appl. Catal. B*, 2011, **107**, 128.
19 H. Q. Wang, Z. B. Wu and Y. Liu, *J. Phys. Chem. C*, 2009, **113**, 13317.
20 *(a)* C. D. Valentin, G. Pacchioni and A. Selloni, *Chem. Mater*., 2005, **17**, 6656; *(b)* X. Chen and C. Burda, *J. Am. Chem. Soc*., 2008, **130**, 5018.
21 S.W. Liu, J. G. Yu and W. G. Wang, *Phys. Chem. Chem. Phys*., 2010, **12**, 12308.
22 *(a)* M. Kruk and M. Jaroniec, *Chem. Mater*., 2001, **13**, 3169; *(b)* X. W. Lou and L. A. Archer, *Adv. Mater*., 2008, **20**, 1853.
23 *(a)* S. Liu, J. Yu and M. Jaroniec, *J. Am. Chem. Soc*., 2010, **132**, 11914; *(b)* J. B. Joo, I. Lee, M. Dahl, G. D. Moon, F. Zaera and Y. Yin, *Adv. Funct. Mater.*, 2013, **23**, 4246; *(c)* S. Han, L. Hu, N. Gao, A. A. Al-Ghamdi and X. Fang, *Adv. Funct. Mater.*, 2014, **24**, 3725.

RSC Advances Accepted Manuscript

This journal is © The Royal Society of Chemistry [year]

Graphic abstract

A novel and unique structure, octahedral bipyramid skeleton, assembled by carbon self-doped TiO_2 flakes with exposed {001} facets was successfully prepared for the first time. These flakes vertically intercross each other and orient the diagonal of the square, assemble into octahedral bipyramid skeleton structure.

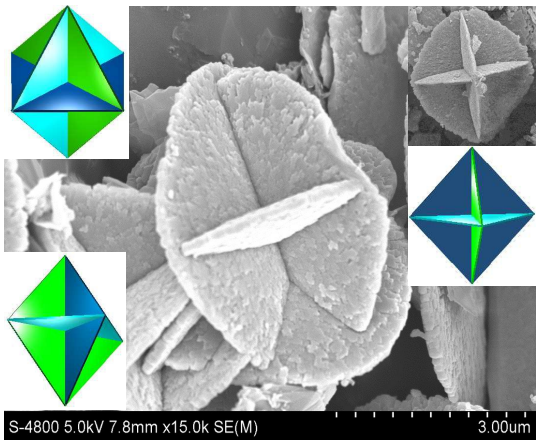

RSC Advances Accepted Manuscript